Computers and Chemical Engineering 127 (2019) 272–281

Contents lists available at ScienceDirect

Computers and Chemical Engineering

journal homepage: www.elsevier.com/locate/compchemeng

Simultaneous measurement uncertainty reduction and proppant bank height control of hydraulic fracturing

Prashanth Siddhamshetty[a,b], Joseph Sang-Il Kwon[a,b,*]

[a] Artie McFerrin Department of Chemical Engineering, Texas A&M University, College Station, TX 77845, USA
[b] Texas A&M Energy Institute, Texas A&M University, College Station, TX 77845, USA

ARTICLE INFO

Article history:
Received 28 March 2019
Revised 6 May 2019
Accepted 15 May 2019
Available online 22 May 2019

Keywords:
Uncertainty reduction
Hydraulic fracturing
Model predictive control
Microseismic monitoring
Proppant bank height control

ABSTRACT

In hydraulic fracturing, higher fracturing fluid injection rates can trigger increased stress, thereby creating more microseismic events; particularly, simultaneously occurring multiple microseismic events can reduce measurement errors. This suggests a new state and output estimation scheme that utilizes the dependence between the fracturing fluid injection rate (i.e., manipulated input) and measurement errors. Motivated by this, we propose a novel control framework for measurement uncertainty reduction while achieving the original control task of proppant bank height control in hydraulic fracturing. Initially, using the simulation data from the high-fidelity model of hydraulic fracturing, a reduced-order model is constructed to design a Kalman filter. Then, a model-based feedback control system is proposed to regulate the uniformity of proppant bank height along the optimal fracture length and achieve accurate state and output estimation by manipulating the fracturing fluid pumping schedule that includes the fracturing fluid injection rate and proppant concentration at the wellbore.

Published by Elsevier Ltd.

1. Introduction

Unconventional resources, generally oil or natural gas resources, are found in ultra low-permeability rock formations, and require specialized extraction techniques such as hydraulic fracturing and horizontal drilling to obtain oil and gas from shale rock formations (Economides et al., 1998; Economides and Nolte, 2000; Bhattacharya and Nikolaou, 2013). Specifically, in hydraulic fracturing highly pressurized fracturing fluids are pumped into shale formations to create fractures. Proppant (e.g., sand, alumina, or zirconia) carried by the injected fracturing fluid into the fractures will hold them open after the hydraulic pressure is removed from the well. After forcefully injecting proppant into fractures and recovering wastewater back, oil and gas will flow more freely towards the well through the created propped fractures (Howard and Fast, 1970).

In hydraulic fracturing, it is important to create fractures with a desired geometry to maximize the oil and gas extraction from unconventional oil and gas reservoirs. To determine the optimal fracture geometry in conventional oil and gas reservoirs, unified fracture design (UFD) was proposed by Economides et al. (2002) for a given amount of proppant to be injected. Recently, Bhattacharya et al. (2012) extended UFD to unconventional oil and gas reservoirs using rock formation properties and the injected amount of proppant. However, in practice, during the planning stage of hydraulic fracturing, the available information regarding rock formation is very limited. Therefore, the use of computationally extensive nonlinear optimization algorithms and complex reservoir simulations (Boulis et al., 2013; Wilson and Durlofsky, 2013; Yu and Sepehrnoori, 2013; Ma et al., 2013) to determine the optimal fracture geometry in unconventional oil and gas reservoirs may not be possible at the planning stage. To overcome these limitations, recently Liu and Valkó (2017) proposed a section-based optimization method by assuming infinity-conductive fractures, which implies that there is no pressure drop inside fractures during the oil and gas production stage, and a constant wellbore pressure is maintained in order to maximize the dimensionless productivity index.

Recently, several efforts have been made to achieve the desired fracture geometry by developing real-time feedback control systems for hydraulic fracturing to regulate suspended proppant concentration for high-permeability reservoirs and proppant bank height for low-permeability reservoirs (Gu and Hoo, 2014; Narasingam et al., 2017; 2018; Sidhu et al., 2018a; 2018b; Yang et al., 2017; Siddhamshetty et al., 2017; 2018a; 2018b; 2019). In these studies, unmeasurable output variables (e.g., average fracture width) and states were estimated using Kalman filters for the purpose of controller design using available measurements. In

* Corresponding author.
E-mail address: kwonx075@tamu.edu (J. Sang-Il Kwon).

https://doi.org/10.1016/j.compchemeng.2019.05.025
0098-1354/Published by Elsevier Ltd.

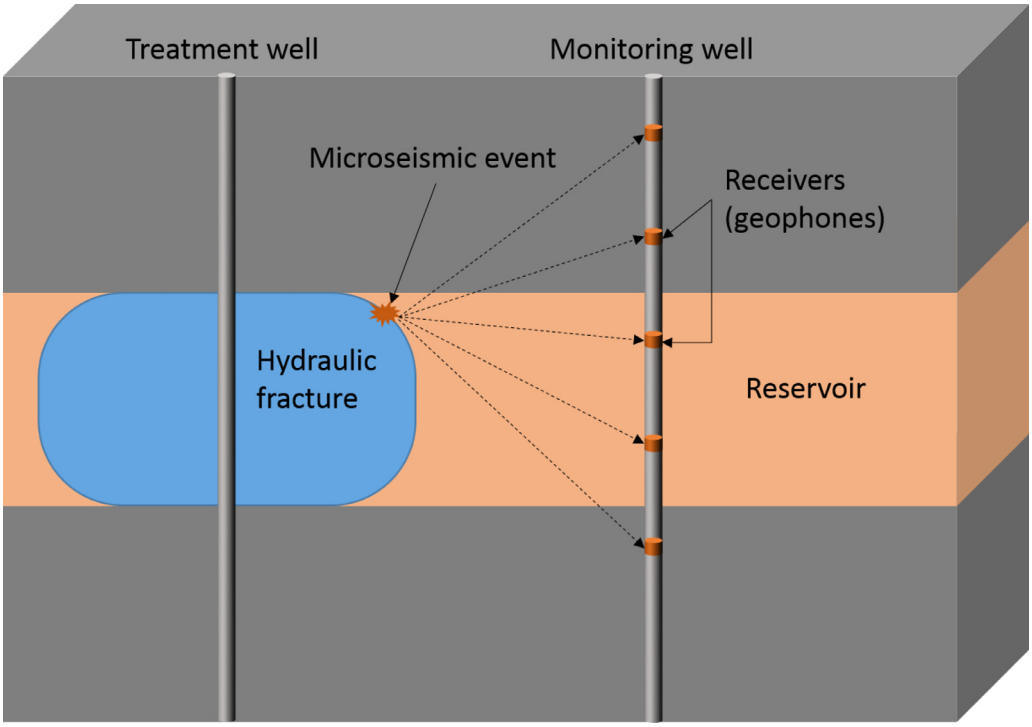

Fig. 1. Schematic of how MSM works.

hydraulic fracturing, among a variety of available measurement technologies, microseismic monitoring (MSM) is the most commonly used one to determine the geometry and location of created hydraulic fractures because it provides the most comprehensive picture of hydraulic fracture growth (Maxwell et al., 2010; Cipolla et al., 2011; 2012).

The principles of MSM are as follows: energy is released due to the cracks propagated in a shale rock formation. This microseismic energy will travel away from the cracks in the form of seismic waves through the surrounding rock formation as shown in Fig. 1 (Clarkson et al., 2012). These seismic waves will temporarily deform the surrounding rock formation when they travel and can be classified into two types: primary (P-) waves, which are the fast propagating waves and secondary (S-) waves, which are the relatively slow propagating shear waves. These microseismic events are then picked up by arrays of accelerometers or three-component geophones which are placed at a nearby monitoring well. Then, the distance between the microseismic event location and the geophone is determined based on the difference in arrival times between primary and secondary waves and a previously calibrated seismic-wave velocity model. Using three or more geophones to detect the same microseismic event location will allow us to determine the location of created fractures in the three-dimensional (3D) space. In general, the measurement uncertainty associated with geophones is very high due to the remote nature of hydraulic fracturing taking place in an underground environment, placing multiple sensors and drilling monitoring wells are required to reduce measurement uncertainty, which is often very expensive.

However, unlike other industrial applications, in hydraulic fracturing the occurrence of measurement depends on the fracturing fluid injection rate at the wellbore (Maxwell et al., 2010). More microseismic events can take place due to increased stress triggered by higher fracturing fluid injection rates. Therefore, creating more microseismic events can reduce measurement errors using MSM. Based on this, Sun et al. (2016) proposed an idea of reducing measurement uncertainty for state and output estimation by manipulating the fracturing fluid injection rate. However, they did not consider regulating the optimal fracture geometry, which can be done by manipulating the same variable. Motivated by this, we propose to develop a model-based feedback control system to reduce the measurement uncertainty while at the same time accomplishing the original control task of achieving the desired fracture geometry at the end of hydraulic fracturing. In this regard, a controller is formulated to minimize the estimation error covariance (uncertainty reduction) as well as the deviation of fracture geometry from its target (set-point tracking).

This paper is organized as follows: in Section 2, we explain the problem statement, and describe the Kalman filter and the relationship between the manipulated input and measurement error covariance. A dynamic model of hydraulic fracturing is described in Section 3. In Section 4, we present the section-based optimization method to obtain the optimal configuration of fractures and wells, and the optimal fracture geometry in unconventional oil and gas reservoirs. In Section 5, we present the development of a reduced-order model (ROM) using the simulation data generated from the dynamic model of hydraulic fracturing, which is then used to develop a Kalman filter for state and output estimation. Next, we introduce a novel real-time model-based feedback control system. The paper concludes with closed-loop simulation results to analyze the performance of the proposed control scheme for simultaneous measurement uncertainty reduction and set-point tracking.

2. Problem statement

In hydraulic fracturing, it is important to achieve a uniform proppant bank height across the optimal fracture length at the end of the process, which will maximize the oil and gas production rates from shale rock formations. In order to obtain the optimal fracture geometry, we propose to design a model-based feedback control system. In the controller, we can estimate unmeasurable states through state estimators such as Kalman filter by utilizing the measurement data available from MSM.

Consider the following state-space representation of a discrete time linear model:

$$x(t_{k+1}) = Ax(t_k) + Bu(t_k) + w(t_k) \tag{1a}$$

$$y(t_k) = Hx(t_k) + v(t_k) \tag{1b}$$

where the input, state, and output variables are represented using $u(t_k)$, $x(t_k)$, and $y(t_k)$, respectively. The random process noise, $w(t_k)$, and measurement noise, $v(t_k)$, are assumed to be derived from a Gaussian distribution with zero mean and covariances Q and R, respectively.

$$w(t_k) \sim N(0, Q) \tag{2a}$$

$$v(t_k) \sim N(0, R) \tag{2b}$$

A Kalman filter consists of two steps: prediction and measurement update steps. Combining these two steps, the formulations for a Kalman filter are presented as follows:

$$\hat{x}(t_{k+1}) = A\hat{x}(t_k) + Bu(t_k) + M(t_k)(y_m(t_k) - \hat{y}(t_k)) \tag{3a}$$

$$M(t_k) = P(t_k)H^T(R(t_k) + HP(t_k)H^T)^{-1} \tag{3b}$$

$$P(t_{k+1}) = (I - M(t_k)H)P(t_k) \tag{3c}$$

$$E(t_k) = HP(t_k)H^T + R \tag{3d}$$

where the notation $\hat{(\cdot)}$ denotes the estimated variables, $M(t_k)$ is the Kalman filter gain, $P(t_k)$ and $E(t_k)$ denote the covariances of the state and output estimation errors, respectively, and the available measurement from the system is denoted using $y_m(t_k)$.

In general, the process and measurement noise information within a Kalman filter is assumed to be known a priori. However, in some systems like hydraulic fracturing, the noise covariance matrices depend on the manipulated input as follows:

$$Q(t_k) = f_w(u(t_k)) \tag{4a}$$

$$R(t_k) = f_v(u(t_k)) \tag{4b}$$

where the nonlinear functions $f_w(\cdot)$ and $f_v(\cdot)$ capture the dependences of covariance matrices on the manipulated input.

In hydraulic fracturing, the occurrence of measurements (i.e., microseismic events) depends on the fracturing fluid injection rate at the wellbore which is an input to the process (Maxwell et al., 2010). More microseismic events will be generated simultaneously due to increased stress and pore pressure triggered by higher fracturing fluid injection rates. The measurement error covariance of simultaneously generated microseismic events can be determined by $R(t_k) = R_{single}/N(t_k)$ where R_{single} is the error covariance of individual measurement and N is the total number of microseismic events per a unit time period. Since N depends on the fracturing fluid injection rate, the measurement error covariance depends on fracturing fluid injection rate at the wellbore which is also the input to the hydraulic fracturing process. Therefore, we have an extra degree of freedom to reduce the measurement uncertainty associated with MSM; otherwise, a high measurement error may lead to incorrect state and output estimation and thereby to a poor controller performance. Therefore, by utilizing this unique dependence of the MSM measurement error on the manipulated input, it is desirable to design a controller to achieve uncertainty reduction as well as set-point tracking.

3. Modeling of hydraulic fracturing

The hydraulic fracturing process model considers fracture propagation, proppant transport, and proppant bank formation.

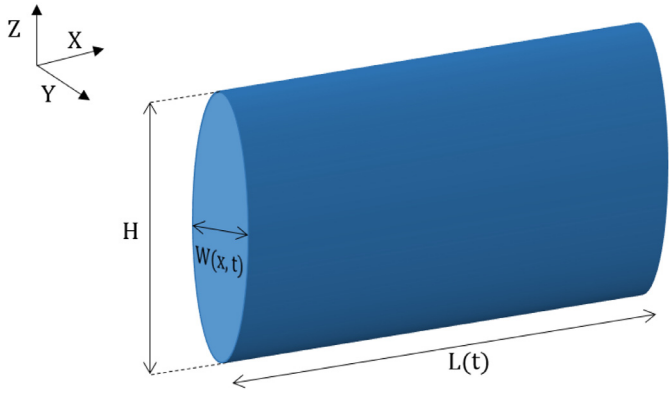

Fig. 2. PKN model.

3.1. Modeling of fracture propagation

In this work, we considered Perkins, Kern, and Nordgren (PKN) model to describe the propagation of a fracture. According to PKN model, fracture propagation exhibits a bi-wing planar shape, which is mirror symmetric with respect to the horizontal wellbore; therefore we model only one of the fracture wings as shown in Fig. 2. Fracture propagation takes place if the fracturing fluid pressure distribution inside fractures is larger than the minimum principal stress in the rock formation and much higher than the fluid pressure inside formation pores; therefore, in order to describe fracture propagation, fluid mechanics and fracture mechanics have to be considered simultaneously. In regard to fluid mechanics, we use the lubrication theory to compute the local fracturing fluid flow rate along the fracture propagation direction, Q_x, for an incompressible Newtonian fluid, which is given below (Nordgren, 1972; Economides and Nolte, 2000):

$$Q_x = -\frac{\pi H W^3}{64\mu}\frac{dP}{dx} \tag{5}$$

where the net pressure, which is obtained by subtracting the minimum principal stress of rock formation from the fluid pressure, is denoted by P, H is the height of fracture which is taken as constant in this work, W is the maximum fracture width which is represented by the minor axis of elliptical fracture as shown in Fig. 2, x represents the fracture propagation direction, and the effective viscosity of fracturing fluid is denoted using μ.

Fracture mechanics is considered using the following elasticity equation, which gives the relationship between the maximum width of elliptical fracture and the net pressure inside the fracture (Sneddon and Elliot, 1946; Gudmundsson, 1983):

$$W = \frac{2PH\left(1-\nu^2\right)}{E} \tag{6}$$

where the Poisson ratio and Young's modulus of formation are denoted by ν and E, respectively.

The injected fracturing fluid will further propagate the fracture into the rock formation, while some of the injected fracturing fluid will leak-off into the surrounding porous rock formation. The conservation of fracturing fluid mass is given by (Nordgren, 1972):

$$\frac{\partial A}{\partial t} + \frac{\partial Q_x}{\partial x} + HU = 0 \tag{7}$$

where the fracture cross-sectional area is given by $A = \pi WH/4$ (Nordgren, 1972), t is the current time, and U is the leak-off rate of fracturing fluid into the porous rock formation which is obtained by Carter's leak-off model (Howard and Fast, 1957; Economides and Nolte, 2000). Essentially, we can obtain the spatio-temporal profiles of fracture width, $W(x, t)$, and length, $L(t)$, by solving Eqs. (5)–(7).

3.2. Modeling of proppant transport and bank formation

During the hydraulic fracturing process, the injected proppant will be carried by the fracturing fluid and settle toward the bottom of fracture because of the gravitational force. The proppant volume concentration, C, inside the fracture can be obtained by the following proppant mass balance equation (Adachi et al., 2007):

$$\frac{\partial(WC)}{\partial t} + \nabla \cdot (WCV_p) = 0 \tag{8}$$

$$C(0,t) = C_0(t) \quad \text{and} \quad C(x,0) = 0 \tag{9}$$

where the vector differential operator is denoted using ∇, the net velocity of proppant particle is denoted by V_p, and the boundary condition needed to solve this equation is given by the proppant concentration injected at the wellbore, $C_0(t)$.

By considering the effect of proppant concentration on terminal settling velocity, the settling velocity of proppant is computed by (Daneshy, 1978):

$$V_s = \frac{(1-C)^2}{10^{1.82C}} \frac{\left(\rho_{sd} - \rho_f\right) g d^2}{18\mu} \tag{10}$$

where the densities of proppant particle and fracturing fluid are denoted by ρ_{sd} and ρ_f, respectively, the gravitational acceleration constant is denoted by g, and d is the proppant particle diameter. The settling of proppant will lead to the formation of proppant bank at the fracture bottom, and the proppant bank height, δ, is given by (Novotny, 1977; Gu and Hoo, 2014):

$$(1-\phi)\frac{d(\delta W)}{dt} = CV_s W, \qquad \delta(x,0) = 0 \tag{11}$$

where the porosity of proppant bank is denoted by ϕ. In unconventional oil and gas reservoirs, because of the use of slickwater which is a low-viscosity fracturing fluid, a significant amount of proppant will be settled, and the formed proppant bank will grow to an equilibrium height at which the rate of proppant washout due to shear force is equal to the rate of gravitational proppant settling. Please refer to Siddhamshetty et al. (2017) for more details regarding how to determine the equilibrium height of proppant bank formation. Essentially, we can obtain the spatio-temporal profiles of suspended proppant concentration, $C(x, t)$, and proppant bank height, $\delta(x, t)$, by solving Eqs. (8)–(11).

4. Optimal configuration of fractures and wells in unconventional oil and gas reservoirs

In this section, we use the section-based optimization method proposed by Liu and Valkó (2017) to determine the optimal number of wells, n_c, number of fractures per each well, n_r, and half-length of fracture, x_f, as this configuration will maximize the productivity of unconventional shale formations for given amounts of fracturing resources. In this work, we fixed the total amount of proppant available for injection as $M_{prop} = 2.38 \times 10^7$ kg, and the resultant optimal values obtained by the section-based optimization method were $n_c = 6$, $n_r = 55$, and $x_f = 120$ m. Please refer to Liu and Valkó (2017) for more details regarding the section-based optimization method.

In unconventional reservoirs, because of the use of slickwater which is a low-viscosity fracturing fluid, the proppant settles quickly forming a proppant bank, which will eventually reach an equilibrium height, h_{eq}. It is very important to achieve this equilibrium height over the required fracture half-length, x_f, which can be translated into achieving the following average fracture width at the end of the hydraulic fracturing process:

$$W_{avg,target} = \frac{M_{prop,frac}}{2\rho_p h_{eq} x_f (1-\phi)} \tag{12}$$

where the total amount of proppant injected to create one fracture is $M_{prop,frac} = 72000$ kg, the proppant particle density is $\rho_p = 2650$ kg/m^3, the porosity of proppant bank is $\phi = 0.61$, the equilibrium height is $h_{eq} = 54$ m for the considered fracturing fluid flow conditions, and the calculated average fracture width at the end of the hydraulic fracturing process is $W_{avg,target} = 5.37$ mm. It is very important to achieve this target average fracture width (set-point for controller design) as it will lead to the optimal fracture geometry for the maximum oil and gas production. However, the measurement of average fracture width is not directly available. Thus, we have to utilize the available measurement of fracture length to estimate the average fracture width using a Kalman filter. In the following section, we will develop a model-based feedback controller to obtain the desired average fracture width at the end of the hydraulic fracturing process and simultaneously reduce the estimation error of average fracture width.

5. Model-based control systems for simultaneous uncertainty reduction and set-point tracking in hydraulic fracturing

In this section, we first construct a ROM of hydraulic fracturing process using the simulation data from the high-fidelity model described in Section 3. MSM is the only reliable measurement technique available during the hydraulic fracturing process, through which we can obtain the real-time measurement of fracture length (Maxwell et al., 2010). Utilizing this available measurement of fracture length and the ROM, we will develop a Kalman filter to predict the average fracture width. As mentioned earlier, the estimation error depends on the measurement noise which is a function of the fracturing fluid injection rate. Based on this, we develop a model predictive controller (MPC) to compute the optimal pumping schedule that will allow us to achieve the desired average fracture width at the end of the hydraulic fracturing process and simultaneously reduce the estimation error associated with the average fracture width.

5.1. Development of ROM

Due to the infinite-dimensional nature of the model described using Eqs. (5)–(11), multi-variable output error state-space (MOESP) algorithm is used to obtain a linear time-invariant state-space model describing fracture propagation and proppant transport phenomena in hydraulic fracturing, which is represented in the following form:

$$x(t_{k+1}) = Ax(t_k) + Bu(t_k) \tag{13a}$$

$$y(t_k) = Hx(t_k) \tag{13b}$$

where the manipulated input variables, $u(t_k) = [Q_{x0}(t_k), C_0(t_k)]^{\mathrm{T}}$, are the injected fracturing fluid flow rate and proppant concentration into the fracture at the wellbore, the output variables, $y(t_k) = [W_{avg}(t_k), L(t_k)]^{\mathrm{T}}$, are the average fracture width and length, and $x(t_k)$ represents the system states. In this work we used a 3$^{\mathrm{rd}}$ order state-space model, and the obtained A, B, and H matrices using MOESP algorithm are given in Eq. (14). We have used the open-loop simulation data generated from the high-fidelity process model to obtain a linear time-invariant state-space model of the hydraulic fracturing process. The training input was designed by taking into account the ranges of allowed input profile (i.e., the minimum and maximum allowable flow rate and proppant concentration). Fig. 3 shows the comparison between the estimated and the actual average fracture width and fracture length with time. It is observed that the estimated average fracture width and fracture length quickly converge to the true values obtained from the

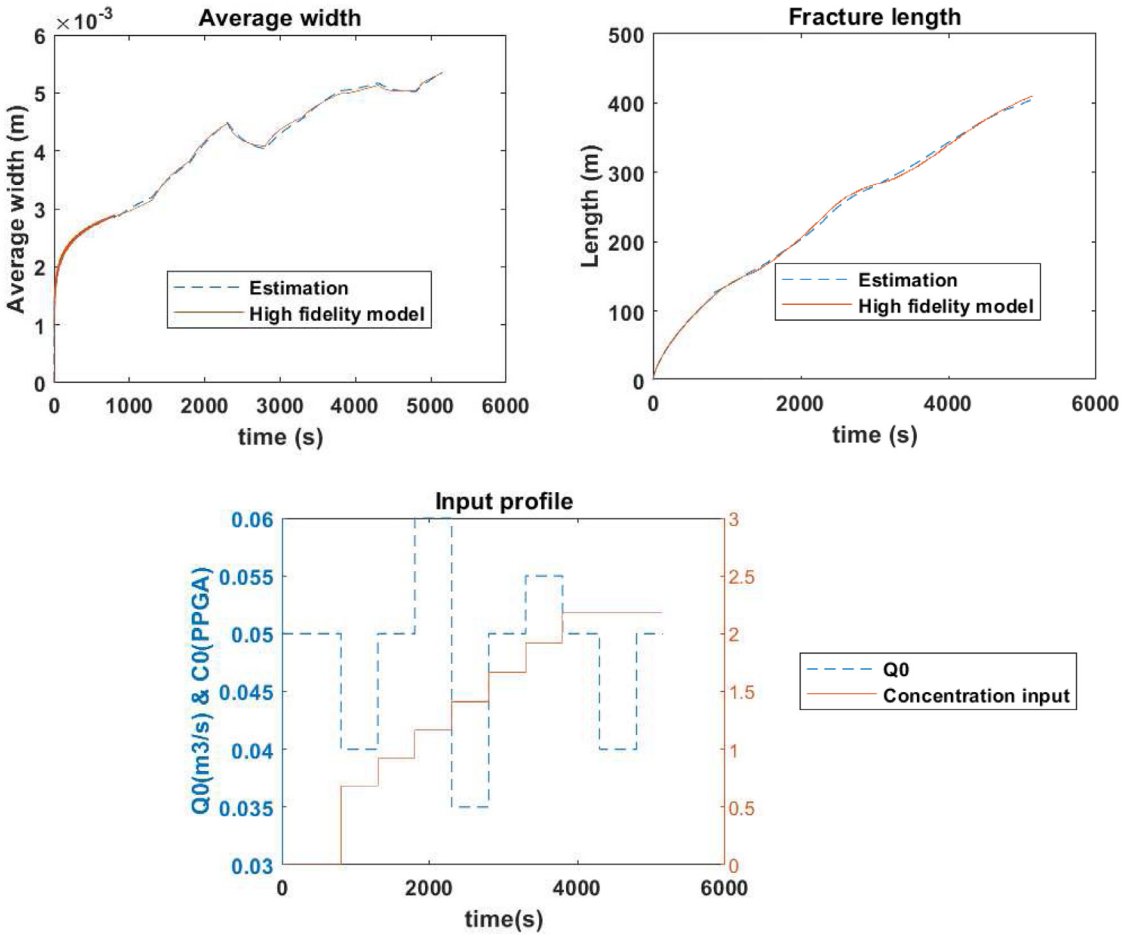

Fig. 3. Comparison between the true values and the estimates of average fracture width and fracture length.

high-fidelity process model.

$$A = \begin{bmatrix} 0.9996 & 1.2434e-04 & -2.3447e-04 \\ 2.010e-04 & 0.9998 & 1.8187e-04 \\ -6.0175e-04 & 2.8465e-04 & 0.9996 \end{bmatrix} \quad (14a)$$

$$B = \begin{bmatrix} 8.4973e-04 & -2.0869e-05 \\ -7.2948e-04 & 3.1820e-05 \\ 0.0011 & 3.6069e-05 \end{bmatrix} \quad (14b)$$

$$H = \begin{bmatrix} 344.8 & -89.7 & 1.1 \\ 1288.5 & -549.1 & -1759.7 \end{bmatrix} \quad (14c)$$

Remark 1. We can also use closed-loop identification methods to obtain a reduced order model as described in Forssell and Ljung (1999) and Kheradmandi and Mhaskar (2018).

Remark 2. In practice, the only reliable measurement during the hydraulic fracturing process is the fracture length. Using this measurement (i.e., $y_m(t_k) = [L(t_k)]$), the average fracture width is estimated through a Kalman filter as described in Section 2.

5.2. Uncertainty reduction

In hydraulic fracturing due to the use of MSM technology, the occurrence of measurement depends on the fracturing fluid injection rate at the wellbore. Higher flow rates are likely to trigger more simultaneous microseismic events because of increased stress and pore pressure resulting from higher fracturing fluid injection rates. The total number of microseismic events per a unit time period, N, is given below:

$$N(t_k) = f_N(Q_{x0}(t_k)) \quad (15)$$

In this work, we assume that two consecutive microseismic events may occur at the same location and time with a same measurement uncertainty (Sun et al., 2016). The measurement error covariance of simultaneously generated microseismic events can be determined by:

$$R(t_k) = R_{single}/N(t_k) \quad (16)$$

where R_{single} is the error covariance of individual measurement. In practice, R_{single} is the error band of single microseismic event uncertainty. By combining Eqs. (15) and (16), the relationship between the fracturing fluid flow rate, $Q_{x0}(t_k)$, and measurement error covariance, $R(t_k)$, is given below:

$$f_v(Q_{x0}(t_k)) = R_{single}/f_N(Q_{x0}(t_k)) \quad (17)$$

Because the covariance of a vector sequence is a matrix, we use the trace (the sum of eigenvalues) of a covariance matrix to evaluate the degree of measurement uncertainty.

5.3. MPC formulations

As indicated by Eqs. (15)–(17), by manipulating the fracturing fluid injection rate, the measurement covariance error and thereby output estimation error can be adjusted as shown in Section 2. Within this regard, a novel MPC is developed to minimize the squared deviation of the average fracture width at the end of the hydraulic fracturing process from its set-point, and the trace value

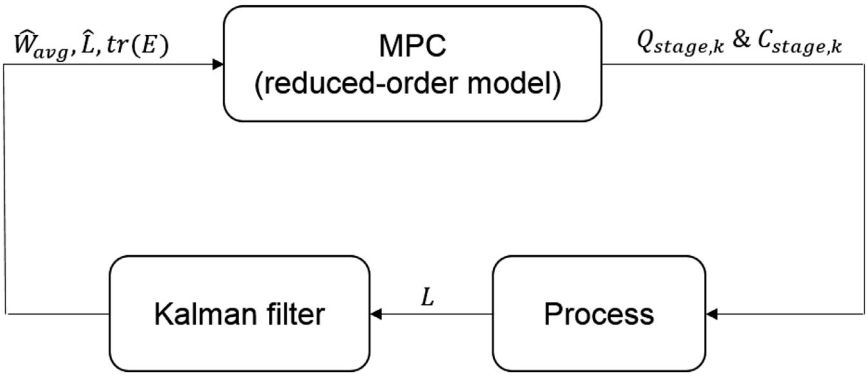

Fig. 4. Schematic of the proposed closed-loop operation.

of the covariance of output estimation error from its desired value, which is given below:

$$\min_{\substack{C_{stage,k},\ldots,C_{stage,9}\\ Q_{stage,k},\ldots,Q_{stage,9}}} (\hat{W}_{avg}(t_f) - W_{avg,target})^2 + Q_c \sum_{i=k}^{9} (tr(E(t_k)) - E_{sp})^2 \tag{18a}$$

$$\text{s.t.} \quad \hat{L}(t_k) = L(t_k) \tag{18b}$$

$$\text{Kalman filter, Eq. (3)} \tag{18c}$$

$$C_{stage,k-1+m} \leq C_{stage,k+m} \leq 2 \text{ PPGA} \tag{18d}$$

$$Q_{min} \leq Q_{stage,k+m} \leq Q_{max} \tag{18e}$$

$$R_{single}(t_k) = 10,000 + 5000 sin(2/(20\pi t_k)) \tag{18f}$$

$$f_N(Q_{x0}(t_k)) = N_0 + 10(Q_{stage,k} - q_0)/q_0 \tag{18g}$$

$$R(t_k) = f_v(Q_{x0}(t_k)) = R_{single}(t_k)/f_N(Q_{x0}(t_k)) \tag{18h}$$

$$m = 1, \ldots, 9 - k \tag{18i}$$

$$\Delta\left(\sum_{k=1}^{9} 2Q_{stage,k}C_{stage,k}\right) = M_{prop,frac} \tag{18j}$$

where Q_c is the weighted norm, the target average fracture width at the end of the hydraulic fracturing process is denoted using $W_{avg,\ target}$, the average fracture width estimated by the Kalman filter of Eq. (18c) is given by $\hat{W}_{avg}(t_k)$, $tr(E(t_k))$ is the trace of the output estimation error covariance matrix, E_{sp} is the desired trace value, $N_0 = 10$ is the number of nominal microseismic events at the fracturing fluid injection rate of $q_0 = 0.035\ m^3/s$, the total process operation time is given by t_f, the period of each sampling time is Δ, the current time is denoted by t_k, the measurements available using MSM is the fracture length, $L(t_k)$, and $C_{stage,k}$ and $Q_{stage,k}$ are the manipulated input variables at the k^{th} pumping stage. The schematic diagram of the proposed MPC is presented in Fig. 4.

In the optimization problem, the only available measurement is the fracture length (Eq. (18b)) and this measurement is used within the Kalman filter to estimate the average fracture width (Eq. (18c)), and the constraints on proppant concentration and fracturing fluid flow rate are considered (Eqs. (18d)–(18e)). The proppant concentration unit is taken as (PPGA), which is 1 pound of the proppant added to one gallon of fracturing fluid. The total amount of proppant injected is constrained using Eq. (18j). The trace of the output estimation error covariance, $tr(E(t_k))$, is given by the Kalman filter using Eq. (3).

Remark 3. The proposed method can be easily extended to account for system nonlinearities by adopting extended Kalman filter techniques, which uses linearized models. By using the input dependent measurement error covariance relationship and extended Kalman filter, we can use the proposed MPC framework for measurement uncertainty reduction while achieving the original control task for nonlinear systems.

Remark 4. There is no desired threshold value on output estimation error covariance and further reducing the error covariance is always beneficial to achieve a better control performance.

6. Closed-loop simulation results under the proposed MPC

In this section, the closed-loop simulation results are presented to demonstrate the performance of the proposed MPC. The high-fidelity model presented in Section 3 was utilized to simulate a hydraulic fracturing process, and the input/output data generated from this model was used to develop a ROM of the process. This ROM was then used to design a Kalman filter for state and output estimation, and subsequently a MPC was designed. In Table 1, the parameter values considered in the high-fidelity process model are provided. The desired average fracture width was $W_{avg,target} = 5.37$ mm. The pad time of $t_p = 800$ s was used. The proposed MPC and the Kalman filter were initialized at $t = t_p$. In the proposed MPC, Δ and t_f values were chosen to be 500 s and 5300 s, respectively, implying that the fracturing fluid pumping schedule consists of 9 stages with the duration of 500 s for each pumping stage. We assumed that the measurement of fracture length, $L(t_k)$, was available at the beginning of each pumping stage (Eq. (18b)). This real-time measurement was then used to predict the unmeasurable state, average fracture width $\hat{W}_{avg}$, via the Kalman filter; then, the output error covariance was predicted. The MPC computed the control input to reduce the measurement uncertainty and simultaneously drive the average fracture width to a desired value at the end of the hydraulic fracturing process.

Table 1
Model parameters used for the simulation.

Parameter	Symbol	Value
formation Young's modulus	E	0.3×10^{10} Pa
formation Poisson ratio	ν	0.2
reservoir thickness	H_r	60 m
proppant particle density	ρ_{sd}	2648 kg/m^3
fracture height	H	60 m
pure fluid density	ρ_f	1000 kg/m^3
viscosity	μ	0.005 Pa · s
settled proppant bank porosity	ϕ	0.61

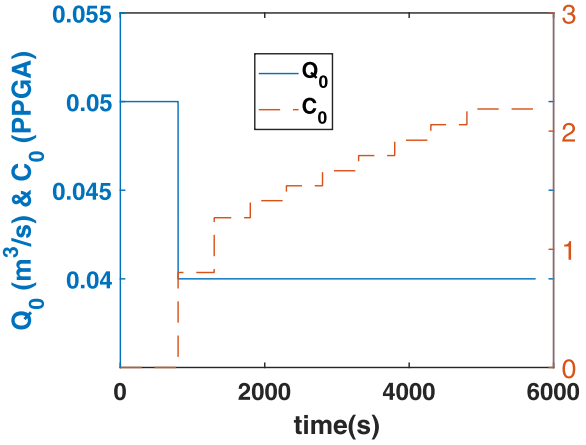

Fig. 5. The fixed pumping schedule used in the first case.

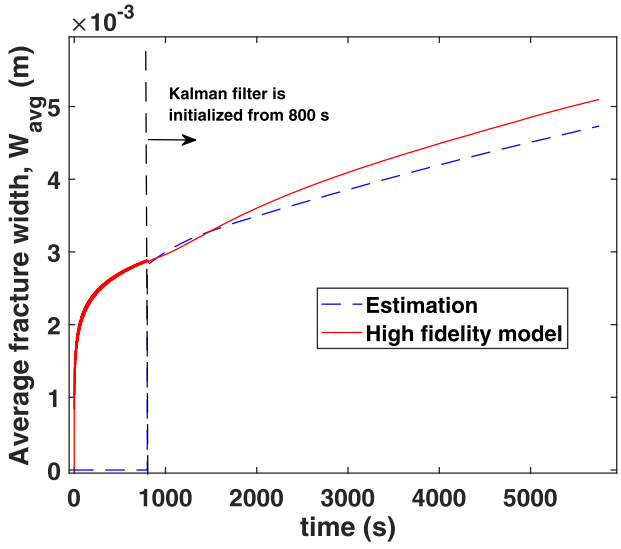

Fig. 6. Average fracture width profile under the fixed pumping schedule.

In this study we examined two cases, where in the first case we considered a fixed fracturing fluid pumping schedule with a constant flow rate and pre-defined proppant concentration profile, and in the second case, the flow rate and proppant concentration were manipulated using the proposed MPC. With the pumping schedule used in the first case (Fig. 5), a discrepancy between the predicted and actual average fracture widths was observed (Fig. 6). The trace of output error covariance, $tr(E)$, is presented in Fig. 7. As shown in Fig. 8, we were not able to achieve the required average fracture width using the fixed fracturing fluid pumping schedule.

In Fig. 9, on the other hand, the average fracture width estimated by the proposed MPC is close to the true value. The pumping schedule obtained by the proposed MPC is shown in Fig. 10. In Fig. 11, it is observed that the proposed MPC can effectively reduce the trace of output error covariance, $tr(E)$. In unconventional reservoirs, because of the use of slickwater which is a low-viscosity fracturing fluid, the proppant settles quickly forming a proppant bank, which will eventually reach an equilibrium height, h_{eq}. With the amounts of resources (e.g., water, proppant and so on) considered in this work, it is very important to achieve this equilibrium height over the required fracture half-length, $x_f = 120$ m, and the desired average fracture width, $W_{avg,target} = 5.37$ mm, at the end of hydraulic fracturing process. Using a fixed fracturing fluid pumping schedule, we were not able to achieve the required average fracture width as shown in Fig. 8, and the proppant

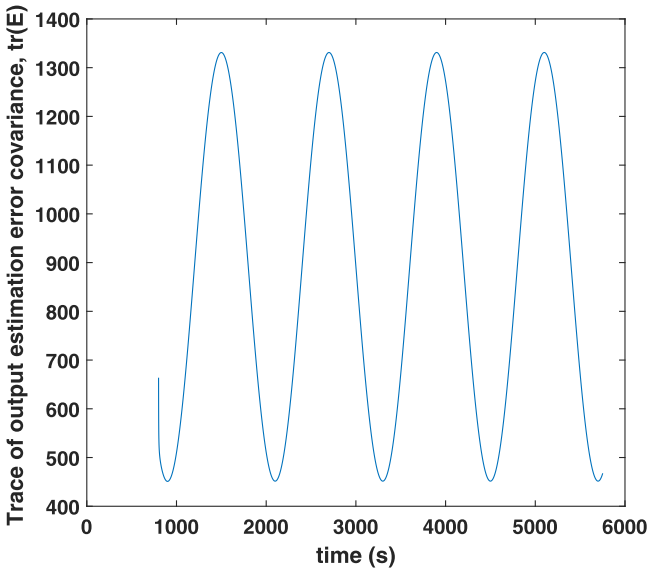

Fig. 7. Trace of output error covariance under the fixed pumping schedule.

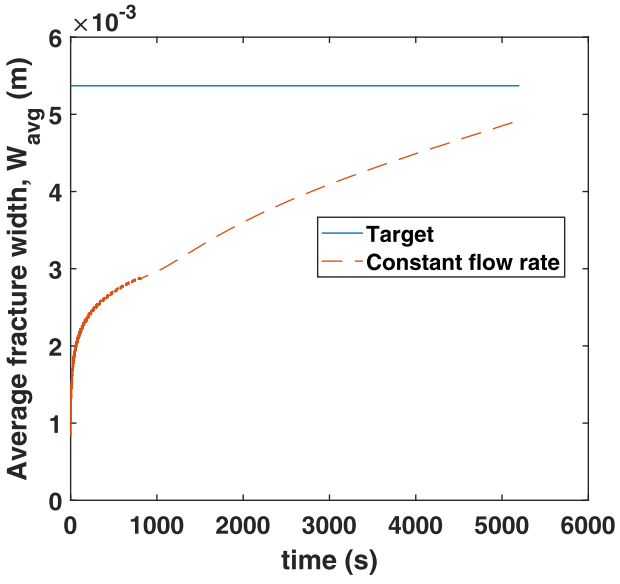

Fig. 8. Average fracture width profile under the fixed pumping schedule compared to its target.

bank height is uniform only for the first 87 m of fracture length as shown in Fig. 12 which is less than the optimal fracture length, and thus, it affects the overall production rate. However, using the proposed MPC, we were able to achieve the desired average fracture width at the end of the process as shown in Fig. 13, and the resultant proppant bank height is uniform across the optimal fracture length, $x_f = 120$ m, as shown in Fig. 14; we have marked the point in Fig. 14 to represent the fracture length covered with the uniform proppant bank height. The fluctuations in Fig. 13 under the proposed MPC is due to the variation in the injected fracturing fluid flow rate as shown in Fig. 10. The growth of average fracture width depends on the interplay between the injected fracturing fluid flow rate and the fracturing fluid leak-off rate into the surrounding porous rock formation. When the fracturing fluid flow rate is dominant it will lead to an increase in the average fracture width; otherwise, it will lead to a decrease in the average fracture width if the fracturing fluid flow rate is less dominant. To demonstrate the proposed MPC's performance, we further extended the

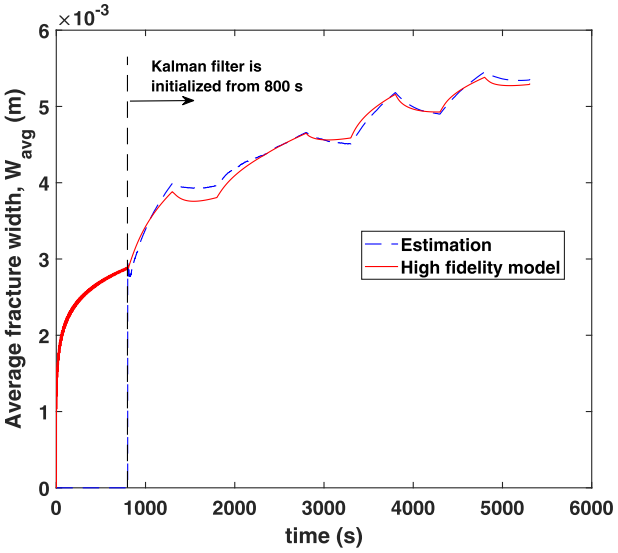

Fig. 9. Average fracture width profile under the proposed MPC.

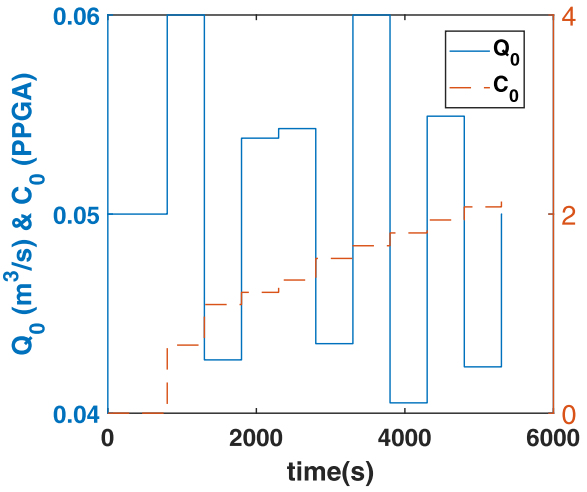

Fig. 10. Pumping schedule computed by the proposed MPC.

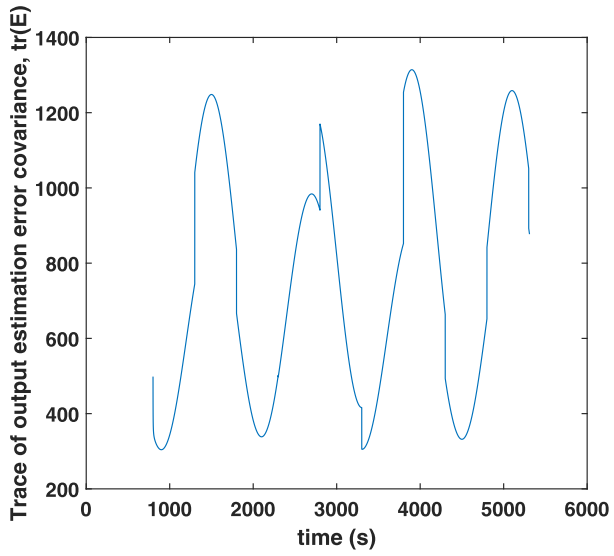

Fig. 11. Trace of output error covariance under the proposed MPC.

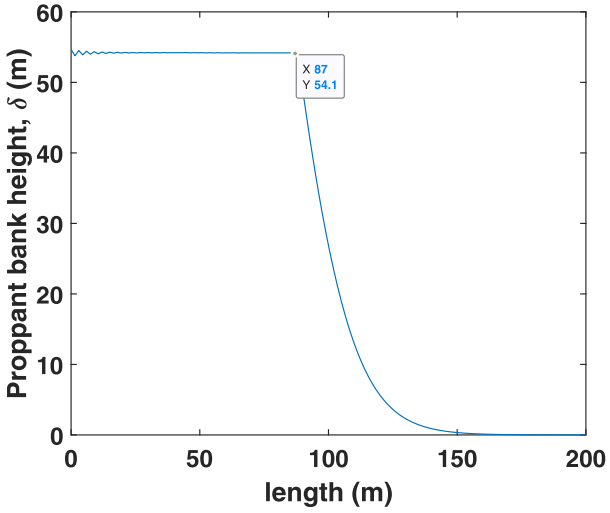

Fig. 12. Proppant bank height at the end of the hydraulic fracturing process under the fixed pumping schedule.

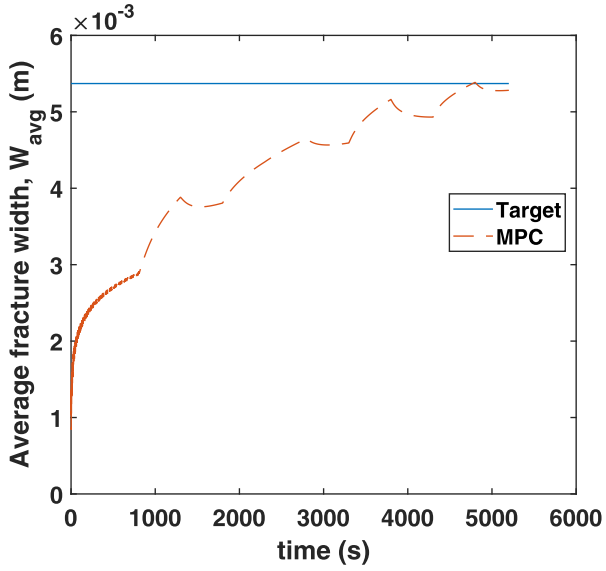

Fig. 13. Average fracture width profile under the proposed MPC.

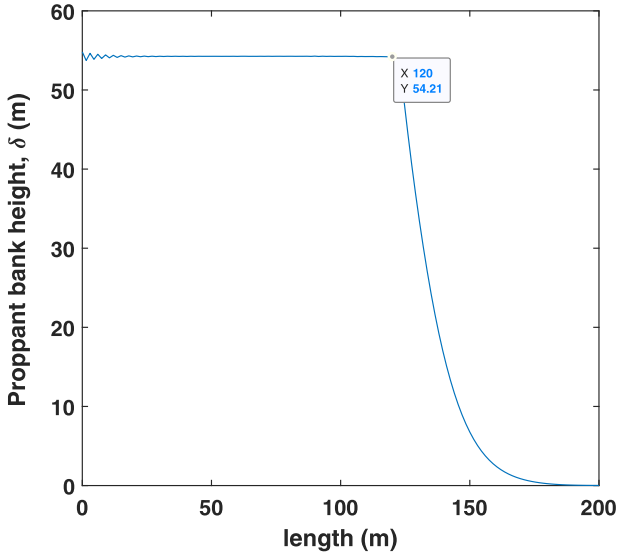

Fig. 14. Proppant bank height at the end of the hydraulic fracturing process under the proposed MPC.

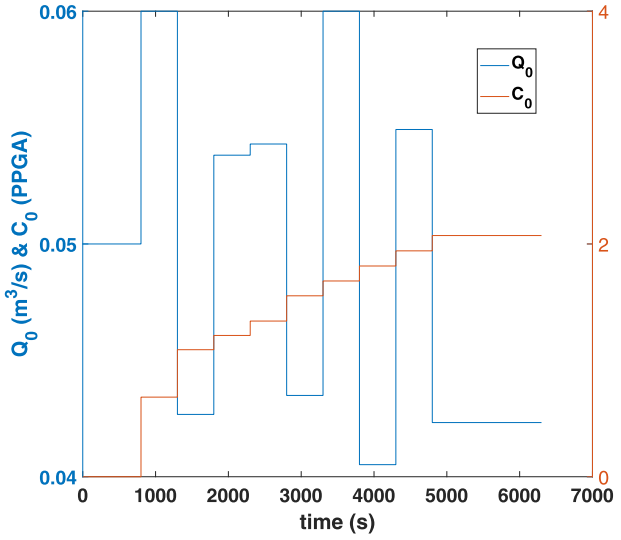

Fig. 15. Pumping schedule computed by the proposed MPC after extending simulation time.

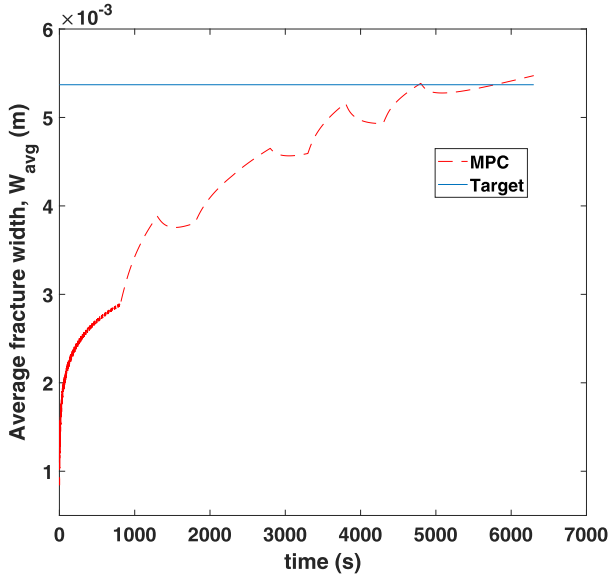

Fig. 16. Average fracture width profile under the proposed MPC after extending simulation time.

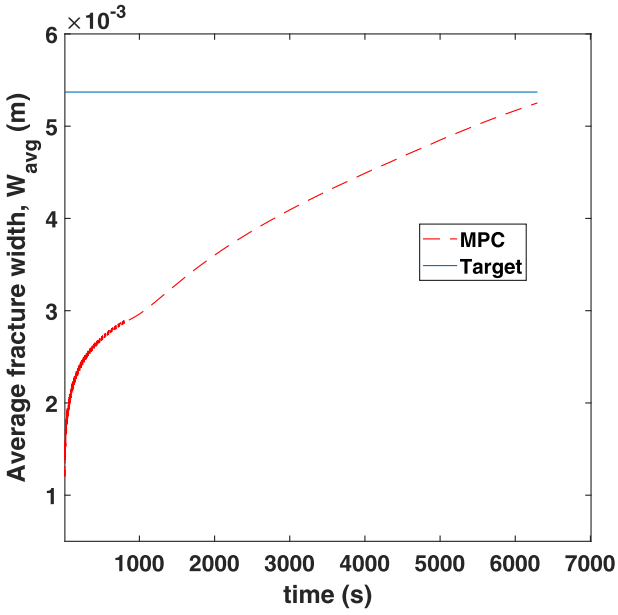

Fig. 17. Average fracture width profile under the fixed pumping schedule after extending simulation time.

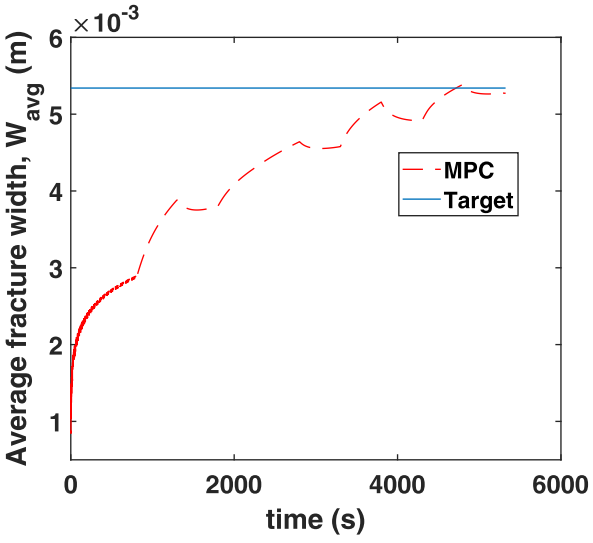

Fig. 18. Average fracture width profile under the proposed MPC when there is a plant-model mismatch in the Youngs modulus with 110% of its nominal value.

total simulation time from 5300 s to 6300 s. Since the output already reached the set-point value, the proposed MPC system tried to maintain the flow rate at its lower bound to decrease the variation in the average fracture width from its set-point value. Because of the constant flow rate in the last three stages (from 4800 s to 6300 s) as shown in Fig. 15, we did not observe any fluctuations in the average fracture width (Fig. 16), which is similar to the case with fixed pumping schedule (Fig. 17).

We studied the effect of a plant-model mismatch in the Young's modulus, *E*, by performing the closed-loop simulations by varying the Young's modulus +/-10% from its nominal value. Using the proposed MPC, the average fracture width at the end of the process is close to the desired value as shown in Fig. 18 even when there is a mismatch in *E*. The performance of the closed-loop system can be further improved when there is a plant-model mismatch by considering offset-free approaches (Wallace et al., 2016).

Comparing the above simulation results for the two cases, it is evident that using the proposed MPC, the output estimation error associated with the average fracture width can be greatly reduced by taking advantage of the relationship between the fracturing fluid injection rate and the frequency of microseismic events; as a result of the accurate estimation of the average fracture width, the desired fracture geometry was also achieved by the proposed MPC. Considering the inaccurate nature of the microseismic sensors, it is very important to accurately estimate states and unmeasurable output variables during the hydraulic fracturing process.

7. Conclusions

In this work, we designed a novel MPC framework to simultaneously reduce the measurement uncertainty in hydraulic fracturing and to achieve the desired average fracture width at the end of the process. The proposed MPC was designed by taking advantage of the relationship between the fracturing fluid injection rate and measurement noise covariance in MSM technique; the most widely used measurement technique for a comprehensive

understanding of fracture geometry. To this end, we initially constructed a ROM using the simulation data generated from the high-fidelity process model, which was then used to develop a Kalman filter for state and output estimation. Utilizing the ROM and Kalman filter, we developed a real-time MPC system to compute the pumping schedule that reduces the measurement uncertainty while at the same time accomplishing the original task of achieving the desired average fracture width, which will lead to the optimal fracture geometry at the end of the process in unconventional oil and gas reservoirs.

Acknowledgments

The authors gratefully acknowledge financial support from the Artie McFerrin Department of Chemical Engineering, the Texas A&M Energy Institute, and the National Science Foundation (CBET-1804407).

References

Adachi, J., Siebrits, E., Peirce, A., Desroches, J., 2007. Computer simulation of hydraulic fractures. Int. J. Rock Mech. Min. Sci. 44, 739–757.
Bhattacharya, S., Nikolaou, M., 2013. Analysis of production history for unconventional gas reservoirs with statistical methods. SPE J. 18 (5), 878–896.
Bhattacharya, S., Nikolaou, M., Economides, M.J., 2012. Unified fracture design for very low permeability reservoirs. J. Nat. Gas Sci. Eng. 9, 184–195.
Boulis, A., Jayakumar, R., Rai, R., 2013. A new approach for well spacing optimisation and its application to various shale gas resources. In: International Petroleum Technology Conference, Beijing,. China
Cipolla, C.L., Mack, M.G., Maxwell, S.C., Downie, R.C., 2011. A practical guide to interpreting microseismic measurements. In: SPE North American Unconventional Gas Conference and Exhibition (SPE 144067), The Woodlands, TX.
Cipolla, C.L., Maxwell, S.C., Mack, M.G., 2012. Engineering guide to the application of microseismic interpretations. In: SPE Hydraulic Fracturing Technology Conference and Exhibition (SPE 152165), The Woodlands, TX.
Clarkson, C.R., Jensen, J.L., Chipperfield, S., 2012. Unconventional gas reservoir evaluation: what do we have to consider? J. Nat. Gas Sci. Eng. 8, 9–33.
Daneshy, A., 1978. Numerical solution of sand transport in hydraulic fracturing. J. Pet. Technol. 30, 132–140.
Economides, M.J., Nolte, K.G., 2000. Reservoir Stimulation. John Wiley & Sons.
Economides, M.J., Oligney, R.E., Valko, P., 2002. Unified Fracture Design. Orsa Press.
Economides, M.J., Watters, L.T., Dunn-Normall, S., 1998. Petroleum Well Construction. Wiley.
Forssell, U., Ljung, L., 1999. Closed-loop identification revisited. Automatica 35, 1215–1241.
Gu, Q., Hoo, K.A., 2014. Evaluating the performance of a fracturing treatment design. Ind. Eng. Chem. Res 53, 10491–10503.
Gudmundsson, A., 1983. Stress estimate from the length/width ratios of fractures. J. Struct. Geol. 5, 623–626.
Howard, G.C., Fast, C.R., 1957. Optimum fluid characteristics for fracture extension. In: Drilling and Production Practices, 24. American Petroleum Institute, pp. 261–270.
Howard, G.C., Fast, C.R., 1970. Hydraulic Fracturing, 02. Henry L. Doherty Memorial Fund of AIME.
Kheradmandi, M., Mhaskar, P., 2018. Model predictive control with closed-loop re-identification. Comput. Chem. Eng. 109, 249–260.
Liu, S., Valkó, P.P., 2017. Optimization of spacing and penetration ratio for infinite conductivity fractures in unconventional reservoirs- a sectional based approach. SPE J. 22, 1877–1892.
Ma, X., Plaksina, T., Gildin, E., 2013. Optimization of placement of hydraulic fracture stages in horizontal wells drilled in shale gas reservoirs. In: In Unconventional Resources Technology Conference. Society of Exploration Geophysicists. American Association of Petroleum Geologists, Denver, CO.
Maxwell, S.C., Rutledge, J., Jones, R., Fehler, M., 2010. Petroleum reservoir characterization using downhole microseismic monitoring. Geophysics 75 (5), 75A129–75A137.
Narasingam, A., Siddhamshetty, P., Kwon, J.S., 2017. Temporal clustering for order reduction of nonlinear parabolic PDE systems with time-dependent spatial domains: application to a hydraulic fracturing process. AIChE J. 63 (9), 3818–3831.
Narasingam, A., Siddhamshetty, P., Kwon, J.S., 2018. Handling spatial heterogeneity in reservoir parameters using proper orthogonal decomposition based ensemble kalman filter for model-based feedback control of hydraulic fracturing. Ind. Eng. Chem. Res. 57, 3977–3989.
Nordgren, R., 1972. Propagation of a vertical hydraulic fracture. SPE J. 12, 306–314.
Novotny, E.J., 1977. Proppant transport. In: SPE Annual Fall Technical Conference and Exhibition (SPE 6813), Denver, CO.
Siddhamshetty, P., Liu, S., Valkó, P.P., Kwon, J.S., 2017. Feedback control of proppant bank heights during hydraulic fracturing for enhanced productivity in shale formations. AIChE J. 64, 1638–1650.
Siddhamshetty, P., Wu, K., Kwon, J.S., 2018. Optimization of simultaneously propagating multiple fractures in hydraulic fracturing to achieve uniform growth using data-based model reduction. Chem. Eng. Res. Des. 136, 675–686.
Siddhamshetty, P., Wu, K., Kwon, J.S., 2019. Modeling and control of proppant distribution of multi-stage hydraulic fracturing in horizontal shale wells. Ind. Eng. Chem. Res. 58, 3159–3169.
Siddhamshetty, P., Yang, S., Kwon, J.S., 2018. Modeling of hydraulic fracturing and designing of online pumping schedules to achieve uniform proppant concentration in conventional oil reservoirs. Comput. Chem. Eng. 114, 306–317.
Sidhu, H.S., Narasingam, A., Siddhamshetty, P., Kwon, J.S., 2018. Model order reduction of nonlinear parabolic PDE systems with moving boundaries using sparse proper orthogonal decomposition: application to hydraulic fracturing. Comput. Chem. Eng. 112, 92–100.
Sidhu, H.S., Siddhamshetty, P., Kwon, J.S., 2018. Approximate dynamic programming based control of proppant concentration in hydraulic fracturing. Mathematics 6 (8), 132.
Sneddon, L., Elliot, H., 1946. The opening of a griffith crack under internal pressure. Q. Appl. Math. 4, 262–267.
Sun, Z., Gu, Q., Dykstra, J., 2016. Uncertainty reduction of hydraulic fracturing process. In: In American Control Conference (ACC), pp. 2135–2141.
Wallace, M., Pon Kumar, S.S., Mhaskar, P., 2016. Offset-free model predictive control with explicit performance specification. Ind. Eng. Chem. Res. 55, 995–1003.
Wilson, K., Durlofsky, L., 2013. Optimization of shale gas field development using direct search techniques and reduced-physics models. J. Pet. Sci. Eng. 108, 304–315.
Yang, S., Siddhamshetty, P., Kwon, J.S., 2017. Optimal pumping schedule design to achieve a uniform proppant concentration level in hydraulic fracturing. Comput. Chem. Eng. 101, 138–147.
Yu, W., Sepehrnoori, K., 2013. Optimization of multiple hydraulically fractured horizontal wells in unconventional gas reservoirs. J. Pet. Eng..